Available online at www.sciencedirect.com
SCIENCE DIRECT
Acta Materialia 54 (2006) 3025–3032
Acta MATERIALIA
www.actamat-journals.com

# Formation of cerium-based bulk metallic glasses

B. Zhang, D.Q. Zhao, M.X. Pan, R.J. Wang, W.H. Wang *

*Institute of Physics, Chinese Academy of Sciences, Beijing 100080, China*

Received 28 October 2005; received in revised form 21 February 2006; accepted 24 February 2006
Available online 11 May 2006

**Abstract**

We report the formation and composition range of Ce-based bulk metallic glasses. Ternary Ce–Al–Cu(Co,Ni) glassy rods of 1–3 mm in diameter can be easily formed in a wide composition range by a conventional copper mold cast method. Substituting Ce with low-cost Ce-rich misch metal (MM), MM–Al–Cu bulk glasses with a similar high glass-forming ability (GFA) can be obtained. With minor addition of extra elements such as Fe, Co, Ni, Nb, Zn and Si, the critical diameter of the full glassy rods of the Ce–Al–Cu matrix can be markedly enhanced from 2 mm to at least 3–10 mm. It is found that the often-cited empirical criteria for bulk metallic glass formation cannot interpret the formation and the addition effect on GFA of the metallic glasses. The striking effect and mechanism of microalloying on the GFA of the metallic glasses are studied. These materials with extremely low glass transition temperatures (341–439 K, even below the boiling temperature of water) and excellent deformability at low temperatures could have potential applications.


*Keywords:* Metallic glass; Alloy

## 1. Introduction

Bulk metallic glasses (BMGs) have attracted much attention due to their considerable scientific and technical importance [1–3]. Compared with polymeric glasses, a similar exploitation of the viscous flow of BMGs is impeded by the higher glass transition temperature $T_g$ and lower resistance to crystallization. However, the mechanical and electrical properties of metallic glasses are, for some applications, far superior to those of polymeric glasses [3,4]. Recently, cerium-based BMGs with an exceptionally low $T_g$ close to room temperature have been developed. Metallic glasses can be repeatedly shaped at low temperatures (such as boiling water temperatures) [5]. Such metallic materials demonstrate that low-temperature malleability in metals is physically possible. Superplasticity at low temperatures has potential applications such as in precise micro-components and thermal mechanical storage [6,7]. From the scientific point of view, BMGs with low $T_g$ close to room temperature provide a model system for investigating the glass transition, slow dynamics in glasses and glass-forming mechanism in metallic alloys.

In this work, we focus on the formation of Ce-based BMGs. We find that ternary Ce–Al–M (M = Cu, Co, Ni) alloys can form full glasses with diameters of 1–3 mm in a wide composition range of 40–80 at.% Ce, 5–25 at.% Al and 10–25 at.% Cu. Replacing Ce by misch metal (MM; a natural mixture of La, Ce, Pr and Nd), MM-based MM–Al–Cu BMGs can also be readily prepared. By selecting appropriate minor additions (about 0.2–3 at.%) of element X (X represents a series of elements such as Fe, Co, Ni, Nb, Si, C and B), quaternary Ce–Al–Cu–X alloys can be easily cast into glassy cylindrical rods with a diameter even larger than 1 cm. All these alloys have an exceptionally low $T_g$ (about 341–439 K) comparable with those typical of polymers such as nylon and PVC [8], and superlasticity in a wide temperature and time window near room temperature. We also find that the glass-forming ability (GFA) of these glass-forming alloys cannot be explained well by some of the often-cited GFA criteria (such as alloys with excellent GFA normally have sufficient atomic radius differences among their components and their composition

* Corresponding author.
*E-mail address:* whw@aphy.iphy.ac.cn (W.H. Wang).

1359-6454/$30.00 
doi:10.1016/j.actamat.2006.02.044

is around the eutectic point) for glass formation [1,9,10]. Ultrasonic measurements reveal the strong atomic interactions in Ce–Al–Cu–X (X = Fe, Co, Ni and Nb) alloys. The striking effect and mechanism of microalloying on the GFA of BMGs are discussed.

## 2. Experimental

The Ce–Al–Cu(Co,Ni), MM–Al–Cu and Ce–Al–Cu–X (X = Bi, Y, Sn, Zr, Mg, Fe, Co, Ni, Nb, Zn, Si, B and C) alloys with the nominal compositions listed in Table 1 were prepared by arc melting pure Al, Cu(Co, Ni) and X with pure Ce or MM in a Ti-gettered argon atmosphere. MM is composed of 22.4 wt.% La, 57.1 wt.% Ce, 4.2 wt.% Pr, 15.6 wt.% Nd and some impurities. The purity of Ce was about 99.5 wt.%, and the other elements had a purity of at least 99.9 wt.%. The alloy ingots were remelted and suck-cast into a Cu mold to obtain cylindrical rods of different diameters ranging from 1 to 10 mm.

The structure of the as-cast alloys was ascertained using X-ray diffraction (XRD) with a MAC M03 XHF diffractometer with Cu Kα radiation and high-resolution transmission electron microscopy (HREM) using a TECNAI-F20 instrument operated at 200 kV. Thermal analysis

Table 1
$D$, $T_g$, $T_x$, $\Delta T_x$, $T_m$,$T_l$, $T_{rg}$ and $\gamma$ for the Ce–Al–Cu(Co,Ni), MM–Al–Cu and Ce–Al–Cu–X (X is the addition element) alloys

| Composition | $D$ (mm) | $T_g$ (K) | $T_x$ (K) | $\Delta T_x$ (K) | $T_m$ (K) | $T_l$ (K) | $T_{rg}$ ($T_g/T_l$) | $\gamma$ [$T_x/(T_g+T_l)$] |
|---|---|---|---|---|---|---|---|---|
| $Ce_{80}Al_{10}Cu_{10}$ | <1 | | | | 647 | 788 | | |
| $Ce_{70}Al_5Cu_{25}$ | <1 | | | | 653 | 670 | | |
| $Ce_{70}Al_{10}Cu_{20}$ | 2 | 341 | 408 | 67 | 647 | 722 | 0.471 | 0.386 |
| $Ce_{70}Al_{15}Cu_{15}$ | 2 | 364 | 406 | 42 | 660 | 686 | 0.470 | 0.356 |
| $Ce_{65}Al_{15}Cu_{20}$ | 2 | 363 | 425 | 62 | 677 | 773 | 0.470 | 0.374 |
| $Ce_{70}Al_{20}Cu_{10}$ | <1 | | | | 666 | 731 | | |
| $Ce_{60}Al_{20}Cu_{20}$ | 3 | 396 | 444 | 48 | 702 | 830 | 0.564 | 0.362 |
| $Ce_{55}Al_{25}Cu_{20}$ | 1 | 439 | 479 | 40 | 744 | 825 | 0.590 | 0.379 |
| $Ce_{40}Al_{40}Cu_{20}$ | <1 | | | | 826 | 834 | | |
| $Ce_{60}Al_{20}Co_{20}$ | 1 | 424 | 468 | 44 | 684 | 798 | 0.531 | 0.383 |
| $Ce_{70}Al_{10}Ni_{20}$ | 1 | 373 | 399 | 26 | 687 | 775 | 0.481 | 0.348 |
| $Ce_{70}Al_{15}Ni_{15}$ | 1 | 368 | 387 | 19 | 691 | 738 | 0.499 | 0.350 |
| $Ce_{68}Al_{10}Cu_{20}Fe_2$ | 5 | 352 | 423 | 71 | 646 | 708 | 0.497 | 0.399 |
| $Ce_{69.8}Al_{10}Cu_{20}Co_{0.2}$ | 8 | 339 | 414 | 75 | 643 | 721 | 0.470 | 0.391 |
| $Ce_{69.5}Al_{10}Cu_{20}Co_{0.5}$ | 10 | 337 | 419 | 82 | 639 | 716 | 0.471 | 0.398 |
| $Ce_{69}Al_{10}Cu_{20}Co_1$ | 10 | 340 | 421 | 81 | 634 | 713 | 0.477 | 0.399 |
| $Ce_{68}Al_{10}Cu_{20}Co_2$ | 10 | 352 | 419 | 67 | 615 | 716 | 0.492 | 0.392 |
| $Ce_{65}Al_{10}Cu_{20}Co_5$ | 8 | 363 | 414 | 51 | 615 | 695 | 0.522 | 0.391 |
| $Ce_{68}Al_{10}Cu_{20}Ni_2$ | 5 | 352 | 421 | 69 | 647 | 710 | 0.496 | 0.396 |
| $Ce_{60}Al_{10}Cu_{20}Ni_{10}$ | 1 | 374 | 441 | 67 | 645 | 672 | 0.557 | 0.422 |
| $Ce_{69}Al_{10}Cu_{20}Nb_1$ | 10 | 352 | 412 | 60 | 646 | 728 | 0.484 | 0.381 |
| $Ce_{68}Al_{10}Cu_{20}Nb_2$ | 8 | 345 | 421 | 76 | 646 | 721 | 0.479 | 0.395 |
| $Ce_{67}Al_{10}Cu_{20}Nb_3$ | 5 | 355 | 404 | 49 | 646 | 723 | 0.491 | 0.375 |
| $Ce_{68}Al_{10}Cu_{20}Y_2$ | <1 | | | | 667 | 721 | | |
| $Ce_{68}Al_{10}Cu_{20}Zr_2$ | <1 | | | | 669 | 743 | | |
| $Ce_{70}Al_{10}Cu_{19}Zn_1$ | 1 | 343 | 391 | 58 | 635 | 743 | 0.462 | 0.360 |
| $Ce_{70}Al_{10}Cu_{18}Zn_2$ | 2 | 345 | 399 | 54 | 633 | 730 | 0.473 | 0.371 |
| $Ce_{70}Al_{10}Cu_{17}Zn_3$ | 3 | 341 | 412 | 71 | 634 | 733 | 0.465 | 0.384 |
| $Ce_{70}Al_{10}Cu_{10}Zn_{10}$ | <1 | | | | 639 | 781 | | |
| $Ce_{70}Al_{10}Cu_{18}Bi_2$ | 1 | 348 | 408 | 60 | 653 | 708 | 0.492 | 0.386 |
| $Ce_{70}Al_{10}Cu_{15}Bi_5$ | <1 | | | | 655 | 746 | | |
| $Ce_{70}Al_{10}Cu_{15}Mg_5$ | <1 | | | | 643 | 744 | | |
| $Ce_{70}Al_{10}Cu_{15}Sn_5$ | <1 | | | | 653 | 698 | | |
| $Ce_{68}Al_{10}Cu_{20}Si_2$ | 3 | 352 | 413 | 61 | 651 | 721 | 0.488 | 0.385 |
| $Ce_{68}Al_{10}Cu_{20}C_2$ | 2 | 352 | 406 | 54 | 650 | 723 | 0.487 | 0.378 |
| $Ce_{68}Al_{10}Cu_{20}B_2$ | 2 | 346 | 393 | 47 | 656 | 731 | 0.473 | 0.365 |
| $MM_{80}Al_{15}Cu_5$ | <1 | – | – | | 666 | 858 | – | – |
| $MM_{70}Al_{15}Cu_{15}$ | 2 | 373 | 436 | 63 | 665 | 795 | 0.469 | 0.373 |
| $MM_{65}Al_{15}Cu_{25}$ | 1 | 390 | 452 | 62 | 675 | 790 | 0.494 | 0.383 |
| $MM_{80}Al_{10}Cu_{10}$ | <1 | – | – | – | 665 | 793 | – | – |
| $MM_{75}Al_{10}Cu_{15}$ | 1 | 378 | 430 | 52 | 660 | 751 | 0.503 | 0.381 |
| $MM_{70}Al_{10}Cu_{20}$ | 1 | 362 | 388 | 26 | 663 | 723 | 0.5 | 0.358 |
| $MM_{67.5}Al_{10}Cu_{22.5}$ | 3 | 360 | 412 | 52 | 680 | 704 | 0.516 | 0.386 |
| $MM_{65}Al_{10}Cu_{25}$ | 2 | 359 | 419 | 60 | 672 | 716 | 0.501 | 0.39 |
| $MM_{62.5}Al_{10}Cu_{27.5}$ | 2 | 372 | 429 | 57 | 663 | 747 | 0.498 | 0.383 |
| $MM_{60}Al_{10}Cu_{30}$ | 1 | 373 | 428 | 55 | 677 | 759 | 0.491 | 0.378 |
| $MM_{67.5}Al_{7.5}Cu_{25}$ | 2 | 347 | 387 | 40 | 667 | 714 | 0.486 | 0.365 |

was carried out using differential scanning calorimetry (DSC; Perkin–Elmer DSC-7) at a heating rate of 10 K/min. Focused ion beam (FIB) etching experiments were carried out using a DB235 FIB etching system. The acoustic velocities were measured using a pulse echo overlap method with a MATEC 6600 model ultrasonic system with a measuring sensitivity of 0.5 ns [11]. The density was determined by the Archimedean technique with an accuracy of within 0.1%. Elastic constants (Young's modulus $E$, shear modulus $G$, and bulk modulus $K$) were derived from the acoustic velocities and the density [11].

## 3. Results and discussion

### 3.1. Ce–Al–Cu(Co,Ni) ternary BMGs

Fig. 1 shows the ternary phase diagram for the composition region of the Ce–Al–Cu BMGs. Five typical bulk glass alloys (filled circles), which can be quenched into a fully glassy state 1–3 mm in diameter, are located in the region. The BMG formation limit is roughly indicated by the alloys (open circles) whose critical fully glassy rod is less than 1 mm in diameter. From Fig. 1, one can see that BMGs with a wide composition range of 40–80 at.% Ce, 5–25 at.% Al and 10–25 at.% Cu can be easily prepared by the copper mold cast method. The as-cast samples were examined using XRD (shown in Fig. 2), HREM (inset in Fig. 2) and DSC (Fig. 3). XRD patterns of the typical $Ce_{55}Al_{25}Cu_{20}$, $Ce_{60}Al_{20}Cu_{20}$, $Ce_{65}Al_{15}Cu_{20}$, $Ce_{70}Al_{10}Cu_{20}$ and $Ce_{70}Al_{15}Cu_{15}$ cast rods have broad diffraction maxima indicating the fully gassy structure of the alloys. The

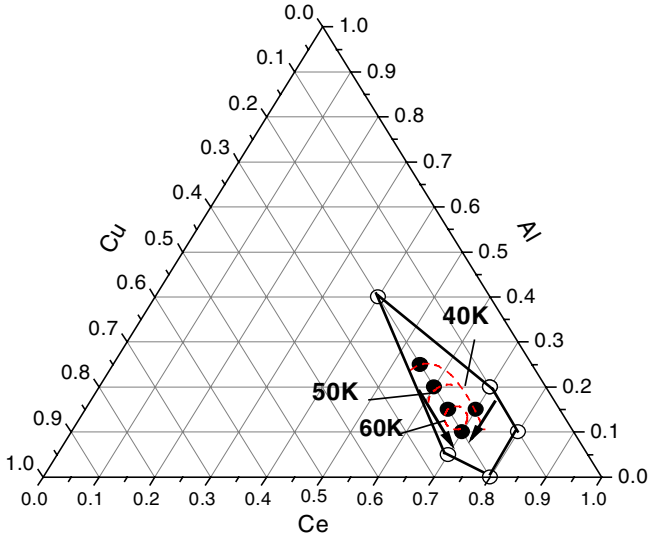


Fig. 1. Ternary phase diagram showing the composition region of Ce–Al–Cu. Filled circles indicate bulk glass formers $Ce_{55}Al_{25}Cu_{20}$, $Ce_{60}Al_{20}Cu_{20}$, $Ce_{65}Al_{15}Cu_{20}$, $Ce_{70}Al_{10}Cu_{20}$ and $Ce_{70}Al_{15}Cu_{15}$; open circles represent poor glass formers $Ce_{40}Al_{40}Cu_{20}$, $Ce_{70}Al_{20}Cu_{10}$, $Ce_{80}Al_{10}Cu_{10}$, $Ce_{80}Cu_{20}$ and $Ce_{70}Al_5Cu_{25}$ (1 mm diameter amorphous rod cannot be cast). The dashed lines show the region for different $\Delta T_x$ values. The solid arrows indicate the decreasing tendency of $T_g$ in the Ce–Al–Cu alloys.

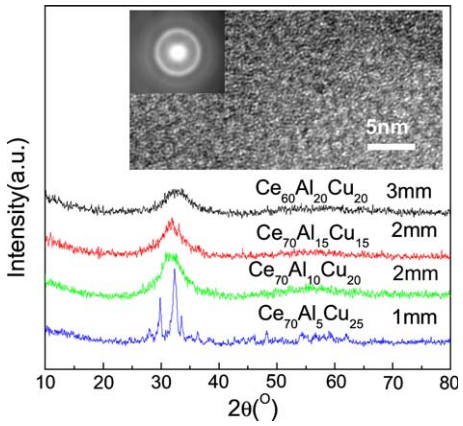


Fig. 2. XRD patterns for the cast rods of $Ce_{60}Al_{20}Cu_{20}$, $Ce_{70}Al_{15}Cu_{15}$, $Ce_{70}Al_{10}Cu_{20}$ and $Ce_{70}Al_5Cu_{25}$ with different diameters. The inset shows the HREM pattern for $Ce_{70}Al_{10}Cu_{20}$ cast sample.

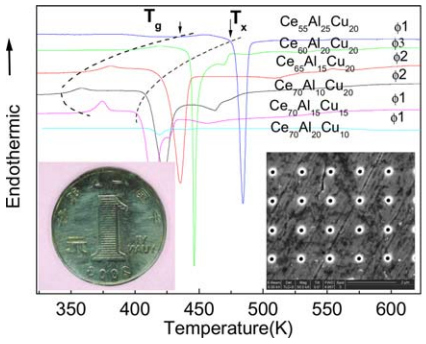


Fig. 3. DSC traces focusing on the glass transition and crystallization of the cast samples of $Ce_{55}Al_{25}Cu_{20}$, $Ce_{60}Al_{20}Cu_{20}$, $Ce_{65}Al_{15}Cu_{20}$, $Ce_{70}Al_{10}Cu_{20}$, $Ce_{70}Al_{15}Cu_{15}$ and $Ce_{70}Al_{20}Cu_{10}$ with different diameters. Insets: one yuan (Chinese coin of 25 mm in diameter) imprinted by hand in nearly boiling water (left) and the $4 \times 5$ array fabricated by FIB technology in the MP001 sample (right).

HREM image of the as-cast $Ce_{70}Al_{10}Cu_{20}$ sample shows a uniform contrast demonstrating the homogenous glassy structure of the alloy. Fig. 3 shows that these as-cast samples have distinct glass transition and sharp crystallization peaks in their DSC patterns, confirming the XRD results. However, for the $Ce_{70}Al_{20}Cu_{10}$ alloy, only a flat line is obtained in the DSC trace for a 1 mm diameter sample indicating partial glassy structure.

As shown in Table 1 and Fig. 3, $Ce_{70}Al_{10}Cu_{20}$ (designated MP001) has the lowest $T_g$ value of 341 K among these BMGs, and the $T_g$ value increases from 341 to 439 K with increasing Al content from 10 to 25 at.% in the $Ce_{80-x}Al_xCu_{20}$ and $Ce_{70}Al_xCu_{30-x}$ systems, indicating that higher Ce content or lower Al content results in lower $T_g$. The solid arrows in Fig. 1 indicate the decreasing trend of $T_g$ in the Ce–Al–Cu phase diagram. Generally, the Ce-based BMGs have exceptionally low $T_g$ (341–439 K) close to that of many polymeric glasses such as nylon (~316 K) and PVC (348–378 K) [8].

The parameter $\Delta T_x$ ($= T_x - T_g$, where $T_x$ is the onset temperature of crystallization) is an often-cited parameter

to characterize the stability and deformability of metallic glasses [1,2]. In contrast to $T_g$, $\Delta T_x$ decreases with increasing Al content in the $Ce_{80-x}Al_xCu_{20}$ system as indicated in Fig. 1, where the dashed lines display the composition-dependent $\Delta T_x$. It decreases from ~60 to ~40 K as the Al content increases from 10 to 25 at.%. In the Ce–Al–Cu system, MP001 has the best deformability because it has the largest $\Delta T_x$ (67 K) among the ternary alloys studied. The low $T_g$ and large $\Delta T_x$ mean MP001 has excellent formability near room temperature. Its thermoplastic behavior in nearly boiling water is demonstrated in Fig. 3. The pattern of a Chinese coin can be easily imprinted on the MP001 sample by hand in nearly boiling water (the left-hand inset of Fig. 3). The results demonstrate the unique viscous state in metallic materials near room temperature. The Ce-based BMGs show high compressive strength (490 MPa) similar to that of some high-strength Al and Mg crystalline alloys [5]. The elastic constants for MP001 are listed in Table 2 The Ce-based BMGs have much higher Young's modulus than that of polymers, while their low $T_g$, similar to that of polymers, means that no more energy is needed for polymer-like imprinting. The right-hand inset of Fig. 3 shows a nano-pit array (200 nm diameter pit at a pitch of 1 μm) in MP001 sample fabricated by FIB etching technology. The precise nanoscale pattern demonstrates that the BMG can be used as a potential material for micro- and nano-manufacturing.

Fig. 4 contrasts the melting behavior of the ternary alloys. $Ce_{70}Al_{10}Cu_{20}$ has the lowest melting temperature ($T_m$) at 647 K while $Ce_{60}Al_{20}Cu_{20}$, the best glass former among the present Ce–Al–Cu alloys, has much higher $T_m$ (702 K) and two separate sharp melting peaks far from the eutectic point (see Fig. 4). For $Ce_{70}Al_5Cu_{25}$, its composition is located very close to the eutectic composition (one sharp melting transformation can be seen in Fig. 4) but it has the worst GFA among the alloys studied (see Fig. 2). These results are not in accord with the eutectic principle for glass formation that has been found useful in many glass-forming alloys [1,9].

Other ternary alloys such as Ce–Al–Ni and Ce–Al–Co can also be formed in the glassy state and their glass-forming compositions are similar to those of the Ce–Al–Cu system. For example, $Ce_{70}Al_{10}Ni_{20}$, $Ce_{70}Al_{15}Ni_{15}$ and $Ce_{60}Al_{20}Co_{20}$ can be readily cast into amorphous rods of at least 1 mm in diameter. The $T_g$ values of these alloys are 373, 368 and 424 K, respectively, as listed in Table 1.

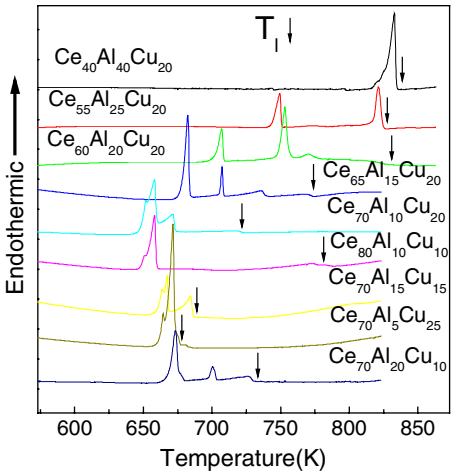


Fig. 4. Melting curves for Ce–Al–Cu alloys at a hearing rate of 10 K/min.

To develop low-cost BMGs, we used MM to replace Ce in the Ce–Al–Cu alloys. The DSC curves focusing on the glass transition and crystallization for as-cast MM–Al–Cu samples are displayed in Fig. 5. The critical glass thickness $D$, $T_g$, $T_x$, $\Delta T_x$, $T_m$ and $T_l$ (the liquidus temperature) for the MM–Al–Cu alloys are collected in Table 1. The MM–Al–Cu alloy system also has as strong a glass-forming tendency as Ce–Al–Cu alloys. The $T_g$ values of these MM-based BMGs ranging from 347 to 390 K are as low as those of Ce–Al–Cu BMGs. The supercooled liquid region $\Delta T_x$ for MM–Al–Cu BMGs is up to 63 K, comparable with that of the Ce–Al–Cu BMGs.

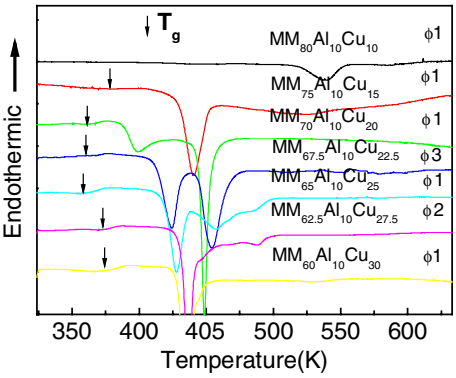


Fig. 5. DSC traces showing the glass transition for MM–Al–Cu cast rods with different diameters.

Table 2
$D$, $\rho$, $V_l$, $V_s$, $E$, $G$ and $K$ for MP001 ($Ce_{70}Al_{10}Cu_{20}$) and alloys with Fe, Co, Ni and Nb addition

| Alloy | $D$ (mm) | $\rho$ (g/cm$^3$) | $\Delta\rho$ (%) | $V_l$ (km/s) | $V_s$ (km/s) | $E$ (GPa) | $\Delta E$ (%) | $G$ (GPa) | $\Delta G$ (%) | $K$ (GPa) | $\Delta K$ (%) |
|---|---|---|---|---|---|---|---|---|---|---|---|
| $Ce_{70}Al_{10}Cu_{20}$ | 2 | 6.699 | 0 | 2.568 | 1.296 | 29.91 | 0 | 11.25 | 0 | 29.18 | 0 |
| $Ce_{68}Al_{10}Cu_{20}Fe_2$ | 5 | 6.740 | 1.06 | 2.646 | 1.316 | 32.70 | 9.3 | 12.32 | 9.5 | 31.35 | 7.4 |
| $Ce_{68}Al_{10}Cu_{20}Co_2$ | 10 | 6.752 | 1.2 | 2.612 | 1.322 | 31.34 | 4.8 | 11.80 | 4.9 | 30.33 | 3.9 |
| $Ce_{68}Al_{10}Cu_{20}Ni_2$ | 5 | 6.753 | 1.3 | 2.659 | 1.332 | 31.93 | 6.8 | 11.98 | 6.5 | 31.77 | 8.9 |
| $Ce_{68}Al_{10}Cu_{20}Nb_2$ | 8 | 6.738 | 1.0 | 2.601 | 1.315 | 30.95 | 3.5 | 11.65 | 3.6 | 30.06 | 3.0 |

Relative changes ($\Delta\rho$, $\Delta E$, $\Delta G$ and $\Delta K$) of $\rho$, $E$, $G$, and $K$ between Fe, Co, Ni and Nb addition alloys and MP001 are also listed.

### 3.2. Superior GFA of Ce–Al–Cu–X BMGs

To further improve the GFA of MP001, a series of elements with different atomic sizes were selected to add into the alloy. According to the atomic radii shown in Fig. 6, these elements can be classified into three groups: large atoms (Goldschmidt radii: Y, 0.182 nm; Bi, 0.182 nm; Zr, 0.16 nm; Mg, 0.16 nm; Sn, 0.158 nm), intermediate atoms (Nb, 0.147 nm; Zn, 0.137 nm; Fe, 0.126 nm; Co, 0.125 nm; Ni, 0.125 nm) and small atoms (Si, 0.115 nm; C, 0.077 nm; B, 0.097 nm) [12]. We find experimentally that the intermediate atoms even with minor addition have the greatest effect on the GFA of the MP001 matrix. Table 1 lists the critical diameter $D$ of the fully glassy Ce–Al–Cu–X (X represents addition elements) alloys. Replacing 2 at.% Ce with Fe, Ni and Nb, the $D$ value of MP001 is drastically enhanced from 2 mm to 5–10 mm. For Co, even a minute trace addition of 0.2 at.% can greatly improve the GFA of MP001 from 2 to 8 mm. On substituting 3 at.% Cu with Zn in MP001, GFA is also increased to at least 3 mm. Fig. 7 shows XRD results of typical glassy rods with different diameters. The XRD patterns of 10 mm diameter rods exhibit only broad diffraction peaks typical for an entirely amorphous structure. The cast samples with different diameters have distinct glass transition and sharp exothermic crystallization peaks in the DSC curves shown in Fig. 8,

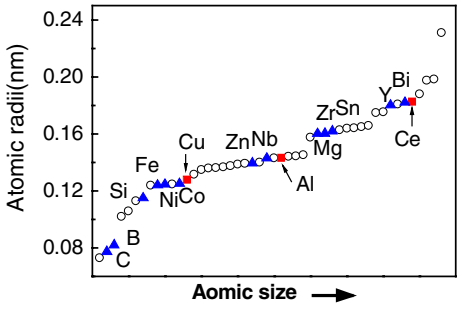


Fig. 6. Atomic sizes of the matrix elements Ce, Al and Cu and addition elements including large atoms Bi, Y, Sn, Zr and Mg, intermediate atoms Fe, Co, Ni, Zn and Nb, and small atoms Si, C and B.

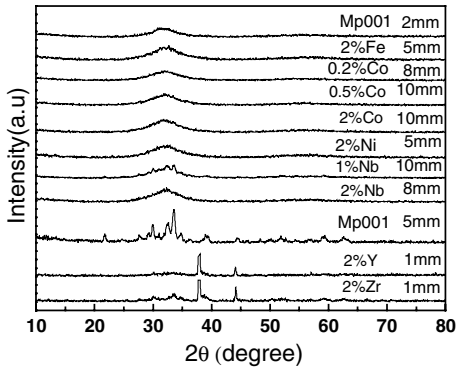


Fig. 7. XRD patterns for the as-cast samples of the MP001 matrix alloy and alloys with Fe, Co, Ni, Nb, Y and Zr additions.

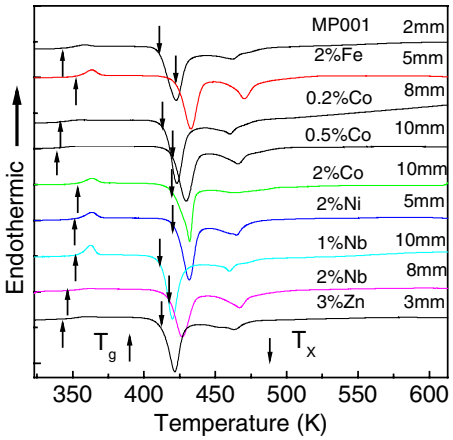


Fig. 8. DSC patterns for the as-cast samples of the MP001 matrix alloy and Fe, Co Ni, Nb and Zn microalloyed alloys.

which supports the XRD results. It should be pointed out that the optimum additive content is below 3 at.%. Fig. 9 displays the "Λ" shape relationship between the GFA and the additive content of Co, Ni, Nb and Zn. Such a phenomenon is rarely seen in the known metallic glasses and contrasts with previous findings that the beneficial addition of transition metals to improve GFA is usually higher than 3 at.% [13]. The thermodynamic parameters $\Delta T_x$, $T_{rg}$ and $\gamma$ for these alloys [1,2,14], which are often used to characterize the GFA of a glass-forming alloy, are collected in Table 1. For Fe, Co, Ni, Nb and Zn microalloyed alloys with excellent GFA, their $\Delta T_x$, $T_{rg}$ and $\gamma$ are nearly identical to those of the MP001 matrix alloy, showing a poor correlation with GFA, as indicated in Fig. 10. For example, $\Delta T_x$ and $\gamma$ of $Ce_{69}Al_{10}Cu_{20}Nb_1$ are 60 K and 0.381, respectively, very close to the value of $\Delta T_x$ (67 K) and $\gamma$ (0.386), respectively, of MP001. The results clearly show that the often-cited parameters $\Delta T_x$, $T_{rg}$ and $\gamma$ are not suitable for characterizing the GFA of these Ce-based BMGs. As shown in Table 1 and Fig. 10, for the glass formers with large $D$ values of 5–10 mm, their $T_{rg}$ values are about 0.471–0.522, which is much smaller than expected for a BMG [1].

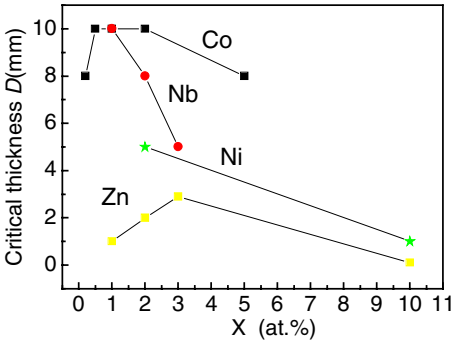


Fig. 9. The "Λ" shape relation between GFA ($D$) and the Co, Ni, Nb and Zn additive content.

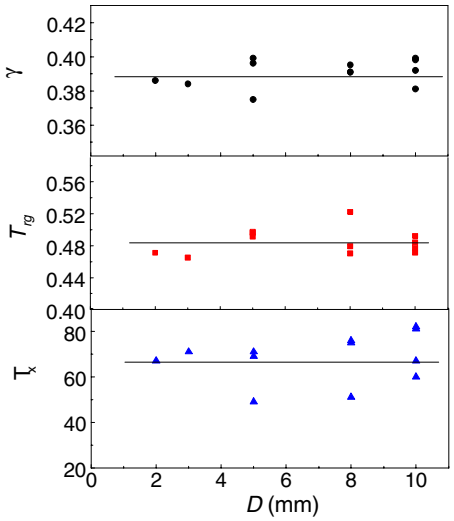


Fig. 10. Dependence of $\Delta T_x$, $T_{rg}$ and $\gamma$ on $D$ for MP001 and the better glass formers with Fe, Co, Ni, Nb and Zn additions.

The melting events of the alloys with minor additions are displayed in Fig. 11. The alloys containing 2% Fe, 2% Ni and 1–2% Nb show nearly the same melting curves as the matrix alloy, suggesting that the minor additions do not significantly change the liquid state of the alloy. This is the main reason that $T_{rg}$ and $\gamma$ for the alloys with Fe, Ni and Nb additions are nearly the same as those of the matrix alloy. For Co microalloying in particular, the melting event splits into separate multiple steps far from eutectic as the Co content increases from 0.2% to 5%. Therefore, the excellent GFA induced by Fe, Co, Ni and Nb addition could not simply be ascribed to the eutectic criterion either.

The positive effect of small atoms on GFA is not as obvious as that of the intermediate atoms. Substituting 2% Ce with Si in MP001 increases its critical size from 2 to 3 mm. The DSC trace for as-cast $Ce_{68}Al_{10}Cu_{20}Si_2$ confirms its improved GFA with 2% Si addition (Fig. 12(a)).

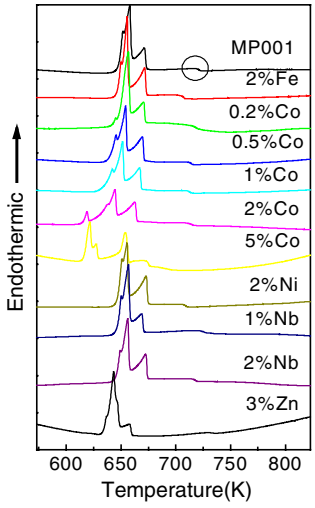


Fig. 11. Melting curves for MP001 and the better glass formers with Fe, Co, Ni, Nb and Zn additions.

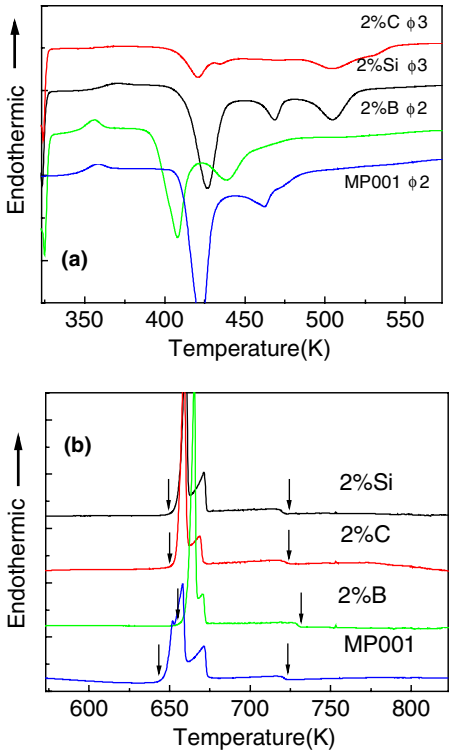


Fig. 12. DSC traces concentrated on the glass transition (a) and melting (b) for MP001 and the alloys with additions of small atoms.

With 2% C and B microalloying, however, the GFA of MP001 is not obviously increased, and 3 mm diameter rods of $Ce_{68}Al_{10}Cu_{20}C_2$ and $Ce_{68}Al_{10}Cu_{20}B_2$ are partially amorphous as indicated in Fig. 12(a). These results are quite different from those of previous studies where more than 2% additions of C, Si and B in Zr-, Cu- and Ni-based alloys are detrimental to the GFA [13,15,16]. The melting events for 2% C, Si and B microalloyed samples are not obviously changed either, as indicated in Fig. 12(b), similar to the situation for addition of intermediate atoms. However, the crystallization process is altered into three stages for the $Ce_{68}Al_{10}Cu_{20}Si_2$ BMG.

Microalloying with the large atom Y can greatly increase the GFA of Fe- and Cu-based alloys [17,18]. However, the addition of large atoms including Y, Zr, Mg, Bi and Sn actually degrades the GFA of the MP001 matrix. As shown in Fig. 7, the XRD curves of as-cast $Ce_{68}Al_{10}Cu_{20}Y_2$ and $Ce_{68}Al_{10}Cu_{20}Zr_2$ rods of 1 mm diameter have sharp diffraction peaks, indicating the poor GFA of the microalloyed alloys. The DSC results for the specimens with Zr, Mg, Bi and Sn additions show no obvious glass transition or crystallization signals (Fig. 13(a)). The addition of large atoms generally increases $T_m$ of the matrix alloy (Fig. 13(b)). Although Mg, Bi and Sn have much lower melting points than Ce, Al and Cu, the alloys containing Mg, Bi and Sn have higher $T_m$. Therefore, minor additions of large atoms of Y, Zr, Mg, Bi and Sn have a negative effect on the GFA of the Ce–Al–Cu alloys.

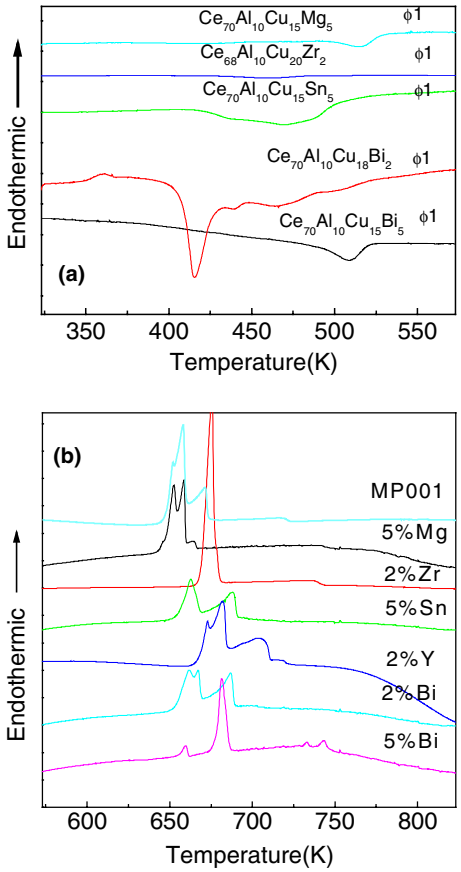


Fig. 13. DSC traces concentrated on the glass transition (a) and melting (b) for the alloys with additions of large atoms.

A large atomic size difference is usually associated with the formation of dense packing structure and the ease of glass formation [12,19]. Zr, Mg and Sn have the optimum atomic size to locate in the atomic size gap between Ce (0.182 nm) and Al (0.143 nm), resulting in more efficient atomic packing and enhanced GFA of the MP001 matrix according to the empirical glass-forming criteria [1–3,10]. However, in fact, they degrade the GFA of alloys on addition of 2%. In contrast, Fe (0.124 nm), Co (0.125 nm), Ni (0.125 nm) and Nb (0.143 nm), whose atomic size is close to that of the main components of Cu (0.128 nm) and Al, favor glass formation in the Ce–Al–Cu alloy. Consequently, atomic size mismatch between constituent elements cannot convincingly explain the marked improvement of GFA by such a small addition of atoms (as low as 2%).

The densities of the alloys with 2% Fe, Co, Ni and Nb addition are listed in Table 2. It is evident that they are about 1–1.3% larger than that of the MP001 matrix. Accordingly, the results confirm that Fe, Co, Ni and Nb additions introduce a substantially more dense packing structure. The measured longitudinal ($V_l$) and transverse ($V_s$) velocities, and Young's modulus ($E$), stress modulus ($G$) and bulk modulus ($K$) are listed in Table 2. The large increases in $V_l$ (1.3–3.89%), $V_s$ (1.5–4.32%), $E$ (3.5–9.33%), $G$ (3.6–9.51%) and $K$ (3.0–7.44%) of the Fe, Co, Ni and Nb microalloyed alloys are also shown in Table 2. The large enhancement of acoustic velocities and elastic constants suggests a much stronger interaction between the local atoms of the glasses and larger resistance of the alloys against stress [11]. Previous X-ray absorption fine structure studies demonstrate that the local bonding for Ce is metallic, while that for Al–Co is covalent characterized by a significant bond length shortening in Al–Co–Ce melt spun metallic glasses [20]. First-principles electronic structure calculations also suggest that covalent bonding is pronounced in Co–Al intermetallic compounds [21]. The particular GFA of the Al-rich Al–Co(Fe)–Ce system has also been derived from the covalent bonding between Al and Co/Fe [22]. Therefore, the strong covalent interaction between Fe, Co, Ni, Nb and the matrix Al might be mainly responsible for the dense packing structure and superior GFA of the microalloyed alloys.

Therefore, from a microalloying technological point of view, the GFA of Ce-based alloys can be enhanced by the following considerations based on the experimental results. An optimum value of the electronegative difference between the additional element and the other components of the alloy can enhance the GFA, because a suitable electronegative difference leads to the formation of quasi-covalence (such as the covalent bonding for Al and Co). Covalent bonding is much stronger than metallic bonding due to the strong attractive interaction, and thus the former is also primarily responsible for the higher degree of atomic packing in the glasses and local strong ordering structure. The ordering leads to a decrease of the configuration entropy $S_c$ of the liquid. According to the Adam–Gibbs theory [23], this will result in a more viscous and higher-density liquid, which slows down the crystallization kinetics on cooling and then enhances the GFA of the alloys.

## 4. Summary

We report that a class of Ce-based Ce–Al–Cu(Ni,Co) BMGs have extremely low $T_g$, wide supercooled liquid region and good GFA in a wide composition range. $Ce_{70}Al_{10}Cu_{20}$ (MP001) has the combined properties of low $T_g$ and large $\Delta T_x$. In the Ce–Al–Cu glass-forming system, an increase of Ce content or decrease of Al content can obviously decrease $T_g$. MM can also be used to prepare cheap BMGs, which have great potential in applications. MM–Al–Cu can also form bulk glasses. We find that appropriate addition of extra elements (such as Fe, Co, Ni, Nb, Zn Si, C and B) can greatly improve the GFA of the Ce–Al–Cu matrix BMG. The strong covalent interaction between Fe, Co, Ni, Nb and the Al matrix is attributed as the reason for the micrioalloying-induced superior GFA of the alloys.

## Acknowledgements

Support from the National Science Foundation of China (Grant Nos. 50321101, 50371097 and 50371098) is

gratefully acknowledged. The experimental assistance of W.P. Cai is appreciated.

## References

[1] Johnson WL. MRS Bull 1999;24:42.
[2] Inoue A. Acta Mater 2000;48:279.
[3] Wang WH, Dong C, Shek CH. Mater Sci Eng R 2004;44:45.
[4] Fred W, Billmeyer JR. In: Textbook of polymer science. New York (NY): Wiley; 1984. p. 3.
[5] Zhang B, Wang WH, Greer AL. Phys Rev Lett 2005;94:205502.
[6] Saotome Y, Zhang T, Inoue A. Mater Sci Eng A 2001;304–306:716.
[7] Marsh G. Mater Today 2003;7:38.
[8] Cardarelli F. Materials handbook. London: Springer; 2000.
[9] Turnbull D. Contemp Phys 1969;10:473.
[10] Greer AL. Nature 1993;366:303.
[11] Schreiber D. In: Elastic constants and their measurement. New York (NY): McGraw-Hill; 1973. p. 35.
[12] Miracle DB, Sanders WS, Senkov ON. Philos Mag 2003;83:2409.
[13] Tan H, Zhang Y, Ma D, Feng YP, Li Y. Acta Mater 2003;51:4551; Zhang J, Tan H, Feng YP, Li Y. Scripta Mater 2005;53:183; Lu ZP, Liu CT. J Mater Sci 2004;39:3965.
[14] Lu ZP, Liu CT. Phys Rev Lett 2003;91:115505.
[15] Wang WH. Intermetallics 2002;10:1249.
[16] Choi-Yim H, Busch R, Johnson WL. J Appl Phys 1998;83:7993.
[17] Xu D, Dan G, Johnson WL. Phys Rev Lett 2004;94:245504.
[18] Lu ZP, Liu CT, Porter WD. Phys Rev Lett 2004;94:245503.
[19] Guo F, Poon SJ. Appl Phys Lett 2003;83:2575.
[20] Mansour AN, Wong CP, Brizzolara RA. Phys Rev B 1994;50:12401.
[21] Mizuno M, Araki H, Shirai Y. Phys Rev B 2003;68:144103.
[22] Hsieh HY, Toby BH, Egami T, Poon SJ, Shiflet GJ. J Mater Res 1990;5:2807.
[23] Adam G, Gibbs JH. J Chem Phys 1965;43:139.